Surface heat flux estimation with embedded fiber Bragg gratings measurements: Numerical study

J. Gaspar, Y. Corre, J-L. Gardarein, M. Firdaouss, D. Guilhem, M. Houry, G. Laffont, C. Niliot, M. Missirlian, C. Pocheau, et al.

Nuclear Materials and Energy 12 (2017) 1077–1081

Contents lists available at ScienceDirect

Nuclear Materials and Energy

journal homepage: www.elsevier.com/locate/nme

Surface heat flux estimation with embedded fiber Bragg gratings measurements: Numerical study

J. Gaspar[a,*], Y. Corre[b], J-L. Gardarein[a], M. Firdaouss[b], D. Guilhem[b], M. Houry[b], G. Laffont[c], C. Le Niliot[a], M. Missirlian[b], C. Pocheau[b], F. Rigollet[a]

[a] IUSTI UMR 7343 CNRS, Aix-Marseille University - 5 rue Enrico Fermi - 13453, Marseille - France
[b] CEA, IRFM, Cadarache 13108 Saint Paul lez Durance, France
[c] CEA, LIST, F-91191 Gif-sur-Yvette, France

ARTICLE INFO

Article history:
Received 16 June 2016
Revised 19 September 2016
Accepted 14 October 2016
Available online 26 October 2016

ABSTRACT

4 probes with Fiber Bragg Gratings (FBGs) will be integrated in Plasma Facing Component (PFC) of the WEST lower divertor in order to measure the bulk temperature distribution in the poloidal direction (11 locations equally spaced). A 2D nonlinear unsteady calculation combined with the Conjugate Gradient Method (CGM) and the adjoint state is used in order to estimate the space and time evolution of the surface heat flux based on temperature measurements. Synthetic measurements are generated assuming optical projection of the heat flux taking into account physical effects such as heat flux decay length (λ_q) and power spreading factor (S) in the private flux region and geometrical effects such as surface chamfering and round leading edges of the component. The inverse method is applied on different synthetic measurements in order to evaluate the ability of using FBG measurements to characterize the heat flux poloidal profile.

1. Introduction

Understanding heat flux deposition processes on Plasma Facing Components (PFC) is essential for PFC designs in order to allow reliable high power steady state plasma operations. One of the main objectives of the WEST (W for tungsten Environment in Steady-state Tokamak) project is to study the behavior of ITER-like actively cooled tungsten (W) Plasma Facing Units (PFU), in order to mitigate the risks for ITER [1]. The ITER-Like PFU should withstand heat fluxes of 10 MW.m^{-2} in steady state. It is therefore necessary to measure these high heat fluxes in order to know their amplitude and spatial distribution on the PFC surface. To achieve these objectives, innovative and ambitious thermal instrumentation as the Fiber Bragg Gratings (FBGs) diagnostic are planned in the WEST lower divertor where the ITER-like components will be integrated.

The first part of the paper describes the FBGs diagnostic. Then, the heat flux estimation methodology with the FBGs measurement is described and tested (Section 3). Finally, the results and the accuracy of the method with synthetics data (based on 3D modelling) are discussed (Section 4).

2. Fiber Bragg gratings diagnostic

2.1. WEST lower divertor

The WEST lower divertor target is located at the bottom of the chamber (Fig. 1a). It is made of 12 independent toroidal sectors of 30°, each composed by 38 PFUs to form a toroidal ring structure. At the start, 11 sectors will be made up of non-actively cooled W coated graphite PFCs (W-coating are 15 µm thick) and only one sector will be a mix of actively cooled ITER-like W PFU and inertial graphite components [2]. The operation with non-actively cooled PFCs is a good opportunity to monitor the temperature with embedded measurements. The inertial target is divided into two Plasma Facing Components (PFCs), one in a Low Field Side (LFS) called the outer PFC and one in the High Field Side (HFS) called the inner PFC. The inertial components will be progressively replaced by the ITER-like W PFU, made of W monoblocks bonded to a copper alloy tube [3].

The divertor X-point configuration allows access to a wide range of plasma equilibrium (changing the X-point height to the target). In this paper we will focus on a particular configuration called Far X-Point (FXP), with X-point localized around 7 cm above the divertor (Fig. 1a). In this configuration the heat flux profile along the poloidal direction is very peaked at the strike

* Corresponding author.
E-mail address: Jonathan.gaspar@univ-amu.fr (J. Gaspar).

http://dx.doi.org/10.1016/j.nme.2016.10.015

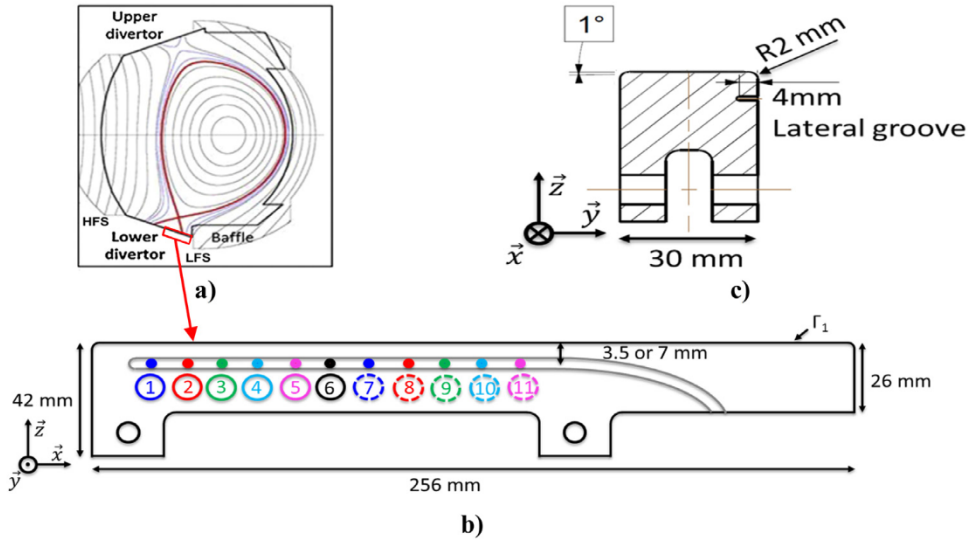

Fig. 1. a) Poloidal magnetic field configuration (Far X-Point) in the WEST Tokamak. **b)** 2D poloidal cross section of the PFC with FBGs (the surface exposed to the plasma is on the top). **c)** 2D toroidal cross section.

point locations (intersections of red line and lower divertor in the Fig. 1a) because of the low magnetic flux expansion. This is the most difficult case for our study.

2.2. Fiber Bragg gratings description

The FBGs are temperature transducer based on a diffraction gratings photowritten by laser into the core of an optical fiber. The FBG advantages is to be immune to electromagnetic interference and to allow the measurement of temperature at different locations on a single fiber with the same footprint than a thermocouple (typically 1 mm in outside diameter). The FBGs are monitored in reflection by a spectrometer (spectral range of 85 nm between 1510 and 1595 nm) with a data acquisition rate of 10 Hz during a pulse. As shown in Fig. 1b each sensing line includes 11 Bragg gratings (length of 3 mm) equally spaced by 12.5 mm in the poloidal direction (typical distance between 2 consecutive ITER-like W monoblocs). The Bragg wavelengths of the gratings have been designed to avoid spectral overlapping during temperature gradient measurement (spectrally spaced allowing maximal ΔT between two successive gratings of 540 °C).

The FBG time-response can be characterized through a simple first order equation giving its step response $u(t)$ defined by $u(t) = 1 - \exp(-\frac{t}{\tau})$ where τ is the time constant defined as the duration required for the sensor to exhibit a 63% change from an external temperature step [4]. In our process operating condition (1 mm sheathed fiber embedded with graphite adhesive) we have $\tau \approx 400ms$ ($\tau \approx 150ms$ for a convective exchange into a water bath). During the heat flux estimation we take into account the FBG time-response by convoluting the temperature calculated at the Bragg gratings locations with the FBG step response $u(t)$ for $\tau = 400ms$.

To test the FBGs capabilities to monitor the PFC temperature, it is planned to install 4 probes with FBGs embedded (in lateral groove of 4 mm see Fig. 1b) in non-actively cooled W-coated graphite PFC of the WEST divertor at 3.5 and 7 mm below the surface (2 at each depth). The FBGs embedded at 3.5 and 7 mm will be named FBG Upper (FBGU) and FBG Lower (FBGL), respectively. The two depths have been selected to investigate different temperature ranges and maximize the heat flux sensitivity of the measurements. At these depths the maximal temperature expected for the FBGs is about 1000 °C, this leads us to use regenerated FBGs [5] which can measure temperature up to 1000 °C.

3. Heat flux estimation methodology

3.1. Inverse heat conduction problem

The Inverse Heat Conduction Problem (IHCP) consists in the determination of the surface heat flux ϕ minimizing the discrepancy between the output of a heat conduction problem (the PFC bulk temperature T) and the temperature measurements provided by the eleven Bragg gratings.

The first step is to define the heat conduction modelling (direct problem) to calculate the temperature history at the FBGs locations depending on the heat flux ϕ absorbed by the PFC. The PFC geometry and dimensions are illustrated in the figures 1b and c where x represents the poloidal direction, y the toroidal direction and z the depth in the PFC. The top surface of the PFC is shaped with a tilt of 1° and round edge of 2 mm on each leading-edge (Fig. 1c). The PFC is made of graphite coated on top and side with a thin tungsten deposit (15 µm). The high heat flux considered in this study leads us to take into account the dependency of the graphite thermal properties with the temperature. The PFC exchanges a radiative heat flux with the surrounding surfaces that are assumed to behave like the blackbody at $T_{rad} = T(t=0)$, the emissivity of the graphite and the W coating is assumed known (respectively $\varepsilon_G = 0.8$ and $\varepsilon_W = 0.3$). Moreover, the WEST chamber is under high vacuum condition during operation (no convection exchanges).

The PFC is initially isothermal (t = 0 s), then the boundary surface Γ_1 is subjected to a heat flux $\phi(x, y, t)$. Furthermore for a single PFC the heat flux on the top surface is quite uniform in the toroidal direction. This leads us to assume the heat transfer problem as a bi-dimensional problem (in x and z Fig. 1b). The principal bias of such assumption is to neglect the round leading-edge (which is close to the FBGs) which is not expected to receive heat flux because of is geometry (optical projection). The accuracy of 2D versus 3D calculations, that enable to save computing time, will be studied in this paper.

The Conjugate Gradient Method (CGM) combined to the adjoint state is the optimization process used to solve the non-linear IHCP. The iterative CGM algorithm (direct, adjoint and sensitivity problem) will not be developed in this paper, the reader can refer to previous work to see the details [6]. The mathematical formulations of the direct, adjoint and sensitivity problems are solved by the finite element method with the software CAST3M.

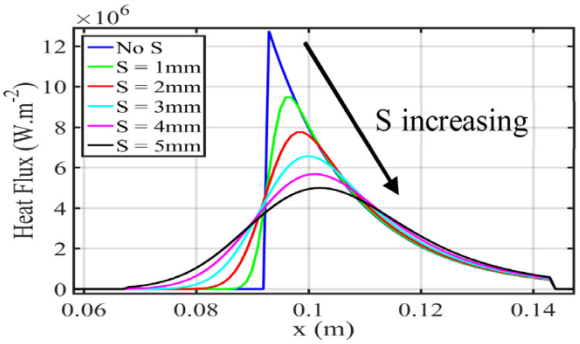

Fig. 2. $\phi(x)$ with $\lambda_q = 5.0$ mm (Eq. 1) with several S values from 0 to 5 mm.

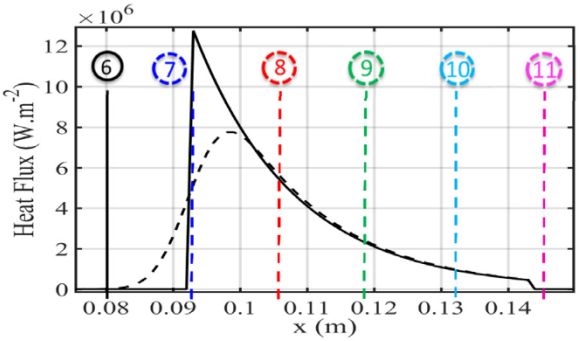

Fig. 3. $\phi_{exact}(x)$ with $\lambda_q = 5.0$ mm (Eq. 1) for: (—) $S \to 0$ mm and (—) $S = 2$ mm with Bragg gratings poloidal locations (vertical lines).

3.2. Heat flux profile

To solve the IHCP we need a priori information on the heat flux and especially on its spatial distribution. Eich et al. showed for the JET and ASDEX divertors [7] that the spatial distribution of the heat flux in the outer side can be expressed by a heuristic formulation, built with IR thermography during Carbon-wall operations, defined by:

$$\phi(x,t) = \frac{\phi_M(t)}{2} exp\left[\left(\frac{S}{2\lambda_q}\right)^2 - \frac{x - x_0}{\lambda_q f_x}\right] erfc \times \left(\frac{S}{2\lambda_q} - \frac{x - x_0}{S f_x}\right) \text{ with } \phi(x > 143 \text{ mm}, t) = 0 \quad (1)$$

where x is the target coordinate, x_0 is the strike point location, λ_q is the power decay length inside the scrape off layer, S is the power spreading factor in the private flux region and f_x is the magnetic flux expansion on the PFC. For the FXP configuration studied here f_x is assumed known and equal to 3. The heat flux is set to 0 for $x > 143$ mm due to the baffle shadowing which intersects the magnetic lines.In our case with the eleven FBGs measurements, we propose to estimate simultaneously the four unknowns: $\phi_M(t)$ the time evolution of the maximal heat flux (when $S = 0$), λ_q, S and x_0 (f_x will be considered known and equal to 3). By the estimation of λ_q and S we can characterize the heat flux spatial distribution from an exponential distribution (when $S = 0$) to a Gaussian distribution (when $S = \lambda_q$) as illustrated in the Fig. 2.

3.3. Accuracy test of the method with 2D modelling

The objective here is to show the accuracy of the present approach in predicting $\phi(x, t)$ with FBGs measurements from a 2D heat conduction modelling. That is the reason why we use the same expression of the heat flux spatial distribution and the same 2D heat conduction modelling to synthetize the measurements and to inverse them (Eq. 1). In order to avoid the "inverse crime" (same model used to synthetize numerical data and to inverse them) we synthetized the measurements by solving the direct problem with the software ANSYS (with different mesh and smaller time step) while we use CAST3M for the estimation. The heat fluxes used to synthetize the measurements are calculated with the Eq. (1) for several values of λ_q (2.5, 5 and 10 mm) and S (no S or $S = 40\%$ of λ_q).

For $\lambda_q = 5$ mm and $S \to 0$ mm (exponential distribution) we choose $x_0 = 93$ mm and $\phi_{max} = 12.75$ MW.m^{-2}. The value of ϕ_{max} is due to the shaping of the graphite PFC which have a tilt of 1° in comparison to the ITER-like PFU (with completely flat surface). Because of this tilt, when the ITER-like PFU is submitted to 10 MW.m^{-2} the graphite PFC receives 12.75 MW.m^{-2} in the FXP configuration. When we change the value of S we keep the heat flux integral constant, this leads different values of ϕ_{max} from 12.75 and 7.75 MW.m^{-2} when S is equal to 0 and 2 mm (see Fig. 3), respectively. The resulting heat fluxes are shown in the Fig. 3.

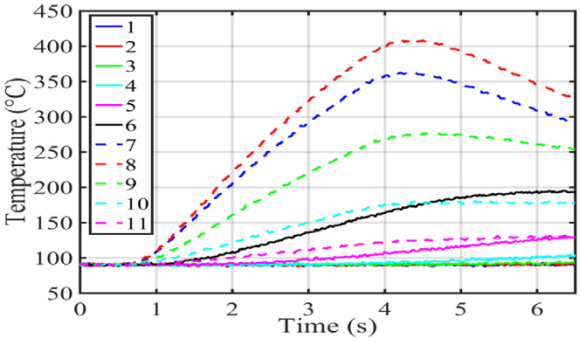

Fig. 4. Temperature simulation performed with ANSYS at FBGL location (embedded at 7 mm) for $\lambda_q = 5$ mm and $S \to 0$ mm with $\tau = 400$ ms and $= 1$ °C .

At $t = 0$ s the PFC is at a uniform temperature $T_0 = 90$ °C. The simulated time is 6.5 s and the time evolution of the imposed heat flux consists in a heating pulse of 3 s (minimum duration in order to reach the thermal equilibrium of the actively cooled ITER-like PFU) starting at $t = 0.5$ s. The Fig. 4 shows the evolution of the noisy temperature (Gaussian distribution with standard deviation $\sigma = 1$ °C) at the Bragg gratings location taking into account the FBGs time response ($\tau = 400$ ms). As expected the Bragg gratings close to the peak heat flux have the maximal heating while the Bragg gratings 1 and 2 have a heating level lower than noise measurement.

We present the results of the inversion using the synthetic measurements for $\lambda_q = 5$ mm and two S values: 1) $S \to 0$ mm and 3) $S = 2$ mm. The initial parameters are set for the two cases to: $\lambda_q = 10$ mm (twice of the exact value), $S = \lambda_q$, $x_0 = 80$ mm and $\phi_M(t)$ is determined with a deconvolution method using the measurements of the Bragg grating 8 with a 1D quadrupole model and Tikhonov regularization [8]. The computational time for a single iteration is about 4 min and the number of iterations needed to converge is about 100. Figs. 5 and 6 show the estimated heat flux dependencies with time and poloidal location x (focused on the heat flux region). We note that the spatial distribution of heat fluxes are well recovered for all cases. The estimated heat flux time evolution shows some oscillations of about 13% around the target values. However, the average during the heating gives a more precise estimate (lower than 5%).

The estimation of λ_q is done with an error less than 2% for all cases and especially for $\lambda_q = 2.5$ mm where the heat flux is the most peaked. We note that when $S \to 0$ mm the estimated value of S is 0.116 mm which is low enough in regard to the mesh size (here 1 mm) to obtain an exponential distribution. Moreover when

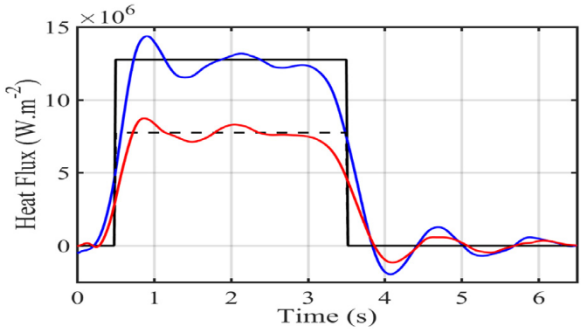

Fig. 5. For $\lambda_q = 5.0$ mm $\phi_M^{exact}(t)$ with: (—) $S \to 0$ mm and (—) $S = 2$ mm. $\phi_M^{estimated}(t)$ with: (—) $S \to 0$ mm and (—) $S = 2$ mm.

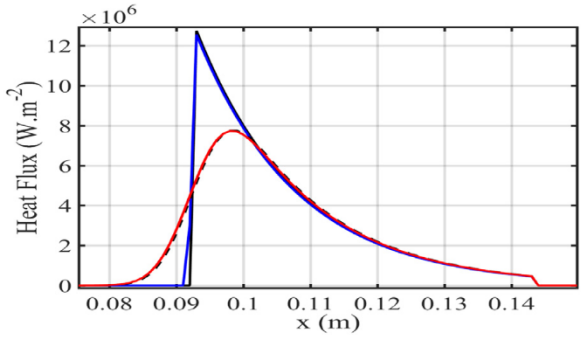

Fig. 6. For $\lambda_q = 5.0$ mm $\phi_M^{exact}(x)$ with: (—) $S \to 0$ mm and (—) $S = 2$ mm. $\phi_M^{mean}(x)$ with: (—) $S \to 0$ mm and (—) $S = 2$ mm. .

$S = 2$ mm, the estimated power spreading factor S is 2.02 mm (low error of 1%) allowing to characterize the spatial distribution of the heat flux in the private flux region. These results show the accuracy of this approach to estimate the intensity of the heat flux and its spatial distribution through the estimation of λ_q, S and x_0 with simplified geometry (no round leading-edge). The same methodology has been applied on synthetic FBGU measurements showing equivalent results with the same order of accuracy on the estimated values.

4. Heat flux estimation results with 3D modelling

The objective of this section is to determine the accuracy of the present approach in predicting $\phi(x, t)$ using a 2D modeling for the inversion with synthetics FBGs measurements generated with a 3D modeling. In this 3D modeling, the surface heat flux $\phi(x, y)$ is the output of the PFCFlux code [2] that takes into account the 3D geometry of the PFC and the magnetic equilibrium.

4.1. Synthetic measurements

The heat flux $\phi(x, y)$ is computed with the PFCFlux code in the FXP configuration for all values of λ_q at the mid-plane and two values of S: $S \to 0$ mm (exponential distribution) and $S = 40\%$ of λ_q (Eq. 1). As described in [2], PFCFlux is a software dedicated to the calculation of the conducted power along the magnetic field lines assuming purely parallel transport (no cross-field transport) from the mid-plane to the PFC surface. Based on ray tracing techniques, it is able to simulate the magnetic shadowing between adjacent PFC's. One of the particularity of this calculation is to take into account the variation of the magnetic field angle of incidence along the PFC which is not taken into account in the Eq. 1. The deposited heat flux map for $\lambda_q = 5$ mm and $S \to 0$ mm is shown in the Fig. 7 with the representation of the poloidal cross section of the 2D modeling (magenta). One can note at the bottom

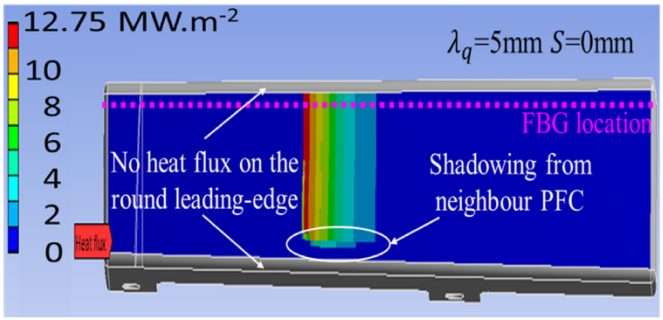

Fig. 7. $\phi(x, y)$ calculated by PFCFlux for $\lambda_q = 5.0$ mm and $S \to 0$ mm at the mid-plane, magenta dotted line is the cross section of the 2D modelling (FBG location). (For interpretation of the references to colour in this figure legend, the reader is referred to the web version of this article.).

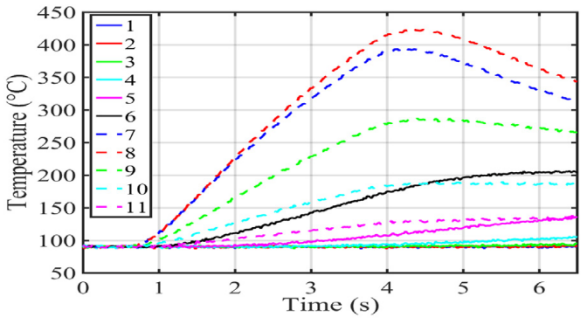

Fig. 8. Temperature simulation performed with ANSYS in 3D at FBGL location for $\lambda_q = 5$ mm and $S \to 0$ mm with $\tau = 400$ ms and $\sigma = 1$ °C.

of the surface the shadowing ($\phi = 0$ in blue) due to the neighbour PFC (about 3 mm bandwidth). In addition, it appears also that the leading-edge of the PFC are not submitted to heat flux due to their 2 mm round edge (result from PFCFlux).

Fig. 8 shows in continuous lines the synthetic measurements generated with ANSYS in 3D using the heat flux computed with PFCFlux with the same time evolution as previously (heating pulse of duration 3 s). As expected the discrepancies between the 3D and 2D modeling (Fig. 4) increase with time. The 3D heating with the same peak heat flux is lower than the 2D one (about 13% after 4 s for the Bragg grating 7) and the cooling rate is higher. This can be explained with the little wetted areas in the 3D modeling due to the shadowing effects and especially for the PFC curved side close to the FBGs location (2 mm round edge with no heat load).

4.2. Estimation results

We present here the results of the inversion using the 3D synthetics measurement for $\lambda_q = 5$ mm with $S \to 0$ mm and $S = 2$ mm. The initial parameters are set as previously: $\lambda_q = 10$ mm, $S = \lambda_q$, $x_0 = 80$ mm and $\phi_M(t)$ with a deconvolution method [8].

Figs. 9 and 10 show respectively the estimated heat fluxes versus time and poloidal location. The pulse dynamic is well recovered despite the underestimation of the intensity especially when $S \to 0$ mm. The error goes to 35% for $\lambda_q = 2.5$ mm with $S \to 0$ mm and is lowers when $S \neq 0$ mm (under 18%), the values are summarized in the Table 1 where ϕ_{mean} is the average of the heat flux at the maximum location for $0.9 < t < 3.1$ s.

The high error when $S \to 0$ mm can be explained by the estimated value of S which is at minimum equal to 0.9 mm (for all λ_q). This minimal value of S is due to the fact that some 3D effects are not taken into account in the inversion modeling (2D heat transfer modeling). The main 3D effect causing this inaccuracy comes from the side of the PFC which are not submitted to

Table 1
Results of the estimation for all λ_q and S for FBGL with 3D synthetic measurements.

	Exact	FBGL	Exact	FBGL	Exact	FBGL	Exact	FBGL	Exact	FBGL	Exact	FBGL
ϕ_{mean} (MW.m^{-2})	12,75	8,36 −34,4%	7,75	6,36 −17,9%	12,75	9,7 −23,9%	7,75	6,56 −15,4%	12,75	10,64 −16,6%	7,75	6,42 −17,2%
λ_q (mm)	2,5	2301 −7,9%	2,5	2281 −8,8%	5	4578 −8,4%	5	4497 −10,1%	10	9476 −5,2%	10	9223 −7,8%
S (mm)	0	0913	1	1297 +29,7%	0	0907	2	2,2 +10,0%	0	0842	4	3,97 −0,8%
x_0 (mm)	93,4	93,31 **−0,1%**	93,4	93,45 **+0,1%**	93,4	93,28 **−0,1%**	93,4	93,65 **+0,3%**	93,4	93,13 **−0,3%**	93,4	94,06 **+0,7%**

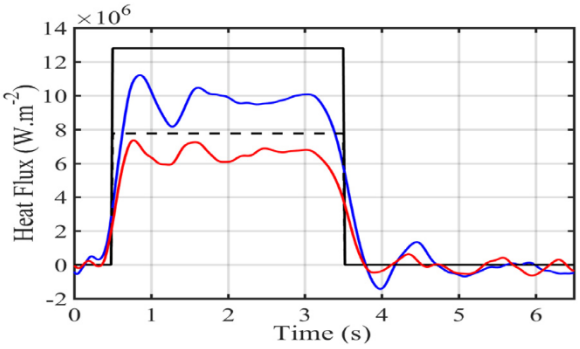

Fig. 9. For λ_q=5.0 mm $\phi_M^{exact}(t)$ with: (—) $S\to 0$ mm and (—) S=2 mm. $\phi_M^{estimated}(t)$ with : (—) $S\to 0$ mm and (—) S=2 mm.

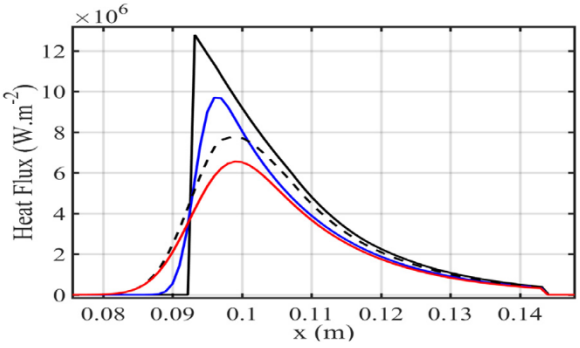

Fig. 10. For λ_q=5.0 mm $\phi_M^{exact}(x)$ from PFCFlux with: (—) $S\to 0$ mm (—) S=2 mm. $\phi_M^{mean}(x)$ with : (—) $S\to 0$ mm and (—) S=2 mm.

heat flux due to their shaping (2 mm round edge) and furthermore the FBGs are embedded very close to this round edge (in lateral groove of 4 mm). This leads to estimate inaccurately the heat flux when its spatial distribution is a pure exponential with no flux in the private flux region. To overcome this inaccuracy it is possible to set S at a prescribed value when $S \leq 0.9$ mm. However for $S \geq 0.9$ mm the error on the heat flux intensity is attenuate and equivalent for all λ_q (from 15 to 18%). Also, the estimation of S is performed with decreasing error from 30% to 1% respectively for S equal to 1 and 4 mm.

Moreover the estimation of λ_q is carried out with error up to 10% unaffected by S value. The increase of the error, in comparison to the previous section (2% in the accuracy test with 2D modelling), can be explained by the fact that our heat flux profile a priori (Eq. 1) does not take into account the variation of the magnetic field angle of incidence on the contrary to PFCFlux. This error could be reduced by modifying the Eq. (1) in order to consider the variation of the magnetic field angle of incidence along the PFC.

5. Conclusion

2D nonlinear unsteady calculations have been used with the Conjugate Gradient Method and the adjoint state, for the heat flux estimation on the divertor graphite PFCs of the WEST tokamak. The combination of the heuristic target heat load profiles [7] with the inverse heat flux calculation using the embedded FBGs data, allows the estimation of the maximum intensity $\phi_M(t)$, the decay length (λ_q), the power spreading factor (S) in the private region and the strike point location (x_0) of the surface heat flux on the divertor PFCs.

After a validation with 2D synthetic data, we have applied the method to synthetics measurement generated with 3D modeling and heat flux $\phi(x, y)$ calculated with a dedicated code (PFCFlux [2]) taking into account surface chamfering and round leading edges of the PFC. The mean heat flux intensity is underestimated from 18% when $S \geq 1$ mm and 35% when $S\to 0$ mm. The results show that the assumptions of our model (2D, heuristic formulation for the spatial distribution of ϕ) lead to acceptable and contained errors on the heat flux estimation as on the decay length estimation (errors on λ_q estimation up to 10% unaffected by S value).

Acknowledgments

This work has been carried out thanks to the support of the A*MIDEX project (n°ANR-11-IDEX-0001-02) funded by the "Investissements d'Avenir" French Government program, managed by the French National Research Agency (ANR).

References

[1] J Bucalossi, et al., Fusion Eng. Des. 89 (2014) 907–912.
[2] M Firdaouss, et al., Fusion Eng. Des. 98-99 (2015) 1294–1298.
[3] M Missirlian, et al., Fusion Eng. Des. 89 (2014) 1048–1053.
[4] B Garnier, et al., Advanced School METTI (Roscoff), 2011.
[5] G Laffont, et al., Measur. Sci. Technol. 24 (2013) 094010.
[6] J Gaspar, et al., Int. J. Therm. Sci. 72 (2013) 82–91.
[7] T Eich, et al., J. Nucl. Mater. 438 (2013) S72–S77.
[8] J-L Gardarein, et al., Inv. Prob. Sci. Eng. 21 (2013) 854–864.